Rev.Adv.Mater.Sci. 21(2009) 139-154

PLASTIC FLOW IN AMORPHOUS COVALENT SOLIDS AND NANOCERAMICS WITH AMORPHOUS INTERGRANULAR LAYERS

M. Yu. Gutkin and I. A. Ovid'ko

Institute of Problems of Mechanical Engineering, Russian Academy of Sciences, Bolshoj 61, Vasil. Ostrov, St. Petersburg, 199178, Russia

Received: June 19, 2009

Abstract. A theoretical model is suggested which describes plastic flow in amorphous covalent solids and amorphous intergranular boundaries in nanoceramics. On the basis of computer simulations (M.J. Demkowicz, A.S. Argon // Phys. Rev. Lett. **93** (2004) 025505), it is supposed that plastic flow in these amorphous structures is carried by liquid-like phase nuclei which form and grow in size within solid-like matrix phase. The nuclei suffer plastic shears modeled as glide dislocation loops. Energetics of formation and growth of the nuclei is examined in bulk amorphous silicon, silicon nitride and nanocomposite *nc*-TiN/a-Si_3N_4 ceramics. Within the model, it is shown that plastic flow in amorphous covalent solids tends to be localized at high stresses and low temperatures. Also, it is revealed that plastic flow within intergranular amorphous layers of a-Si_3N_4 in nanocomposite *nc*-TiN/a-Si_3N_4 can initiate cracks whose equilibrium and critical (Griffith) lengths depend on grain size and temperature.

1. INTRODUCTION

Nanocrystalline metallic and ceramic materials exhibit the outstanding mechanical properties highly attractive for a wide range of applications; see, e.g., [1-18]. In particular, nanocrystalline ceramic bulk materials and coatings are often characterized by superstrength, superhardness and good wear resistance [11-18]. These properties are strongly influenced by intergranular boundaries which often have the amorphous covalent structure and occupy very large volume fractions in nanocrystalline specimens; see, e.g., experimental data [16-18] and computer simulations [19,20]. In this context, there is rapidly growing interest in understanding micromechanisms for plastic flow in amorphous intergranular boundaries of nanoceramics and their "model" bulk analogs, the namely amorphous bulk solids with covalent bonds (heareinafter called amorphous covalent solids). In particular, recently Demkowicz and Argon [21-23] have used computer simulation to study the structure and mechanical behavior of amorphous silicon. They have shown that the structure is composed of regions of liquid-like and solid-like material. Depending on the velocity of solidification of liquid silicon in producing the amorphous state, the volume fractions of the liquid-like and solid-like materials change. Deviation in the liquid-like and solid-like fractions leads to changes in regimes of plastic flow. When the liquid-like fraction increases, the plastic flow becomes more homogenous. Moreover, the liquid-like fraction grows under mechanical loading. The authors [21-23] have concluded that the regions of liquid-like material are the carriers of plastic flow in amorphous silicon. Since it is a typical example of amorphous covalent solids, Demkowicz and Argon [22] have suggested that these features are also characteristic of other amorphous covalent struc-

Corresponding author: M.Yu. Gutkin, e-mail: gutkin@def.ipme.ru

tures, in particular, of the amorphous intergranular layers of Si_3N_4 between the TiN nanocrystallites in *nc*-TiN/a-Si_3N_4 ceramic nanocomposites. Using computer simulation, Demkowicz et al. [24] have observed the formation and development of regions of liquid-like phase in grain boundaries at plastic deformation of nanocrystalline silicon.

In the present work, based on the results of computer simulations [21-24], we suggest a micromechanical model of plastic flow in covalent amorphous materials and apply it to the case of intergranular layers of Si_3N_4 in *nc*-TiN/a-Si_3N_4 ceramic nanocomposites. We show that the initial plastic flow in favorably oriented intergranular layers can stimulate either plastic flow or crack generation in neighboring intergranular layers, depending on temperature and grain size.

2. MODEL

A micromechanical model for structure of amorphous silicon under an external tensile stress σ is shown in Fig. 1. Following Demkowicz and Argon [21-23], we assume that the external loading leads to formation of nuclei of liquid-like material in the matrix of solid-like material. The nuclei are supposed to have the shape of oblate ellipsoids oriented along the maximum resolved shear stress $\tau = \sigma/2$. Every nucleus suffers a plastic shear by a vector ***s*** due to its liquid-like structure. On the other hand, this plastic shear is localized inside the nucleus, in which case it is effectively described by a glide dislocation loop with the Burgers vector ***s***. For the sake of simplicity of the following calculations, we consider the loop to be rectangular in shape. Within our model, both the dimensions of the nucleus and loop synchronously increase under external loading. Moreover, the Burgers vector ***s*** of the loop (hereinafter we call its magnitude 'the loop strength *s*') increases, too. In other words, under the action of an external shear stress τ, the amorphous material is subjected to homogeneous nucleation and extension of glide dislocation loops of increasing strength *s* (from zero) which are encapsulated into ellipsoidal inclusions of liquid-like material. (These processes are similar to local shear events in metallic glasses [25]. Also, nucleation and extension of glide dislocation loops in amorphous covalent structures are similar to processes of nucleation and extension of nanodisturbances, "non-crystallographic" partial dislocation loops (characterized by tiny Burgers vector magnitudes) that bound generalized stacking faults in crystalline solids [26-29]. Nucleation

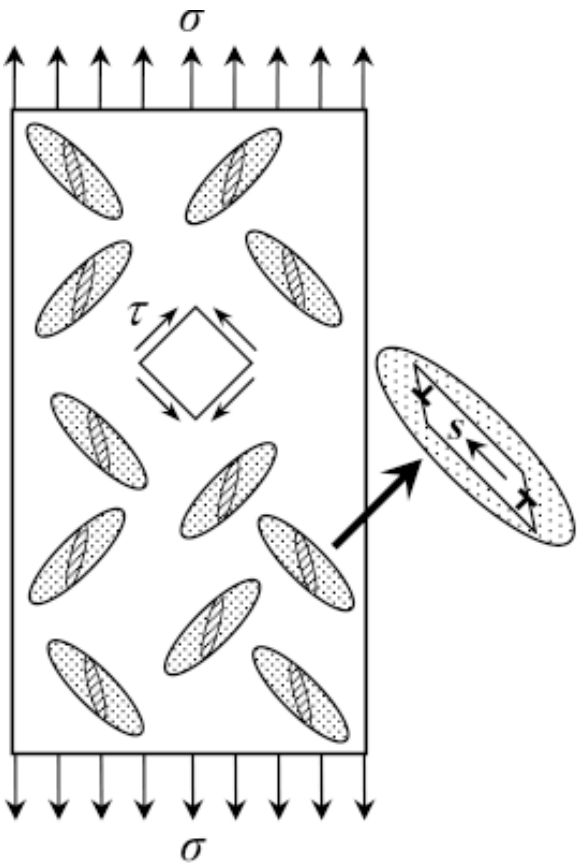

Fig. 1. Model for homogeneous generation of plastic flow in covalent amorphous solids. Local shear events are treated through glide dislocation loops of strength (Burgers vector) ***s***, which are surrounded by ellipsoidal regions of liquid-like phase having smaller shear moduli.

of nanodisturbances and their transformations into conventional "crystallographic" partials have been recently observed in "in-situ" experiments during plastic deformation of special titanium alloys [29].)

Consider the change in the total energy of the system ΔW per one nucleus containing a dislocation loop. In the framework of our model it is given by

$$\Delta W = W_L + HV - \tau s S, \qquad (1)$$

where W_L is the strain energy of a rectangular glide dislocation loop, H is the excess enthalpy of the liquid-like phase of the amorphous material relative to its solid-like phase, V is the volume of the liquid-like phase nucleus surrounding the dislocation loop, and S is the area of the dislocation loop. In writing formula (1), we did not take into account the elastic interaction between dislocation loops.

This approach is correct because the loop dimensions are always smaller than or equal to the space between the loop centers in the model, in which case the energy of elastic interaction between two neighboring loops is much smaller than the self strain energy of a loop.

Let a dislocation loop have the dimensions $p \times q$, and its Burgers vector $\boldsymbol{s}$ is oriented along the segments of length p. Then the strain energy of the loop W_L reads [30]

$$W_L = \frac{Gs^2}{2\pi(1-\nu)}\left\{(1-\nu)(r-p-q) + q\left(1+\ln\frac{2pq}{r_c(r+q)}\right)+p(1-\nu)\left(1+\ln\frac{2pq}{r_c(r+q)}\right)\right\}, \quad (2)$$

where G is the effective shear modulus of the composite materials consisting of the solid-like phase (matrix) and liquid-like phase (oblate ellipsoidal inclusions), ν is the effective Poisson ratio of the composite, $r = \sqrt{p^2+q^2}$, and $r_c \approx s$ is the cut-off radius for the stress field of the dislocation loop near its line. This formula is correct when $p,q > r_c$.

The effective elastic moduli of the composite can be estimated as follows. Let the inclusions, which have the moduli different from those of the matrix, be randomly distributed in the matrix. Let every inclusion be contained in the matrix cubic cell of dimension λ, and these cells occupy the whole material without voids and intersections. In our model, the inclusions are oriented along four different directions where the resolved shear stress is maximum, in which case we can approximate their orientation to be close to random. Therefore, the effective shear modulus of such a composite can be approximated by the well known formula [31]

$$G = G_m - c\frac{(G_m+\eta G_i)(G_m-G_i)}{G_i(1+\eta)}, \quad (3)$$

where G_m and G_i are the shear moduli of the matrix and inclusion, respectively, $c << 1$ is the volume fraction of inclusions, $\eta = 0.5(7 - 5\nu_i)/(4 - 5\nu_i)$, and ν_i is the Poisson ratio of the inclusion. The inclusion volume V is approximated by the area of the dislocation loop, $S = pq$, multiplied by some effective thickness t of the inclusion: $V \approx pqt$. Then the volume fraction of the inclusions is estimated by $c = V/\lambda^3 \approx pqt/\lambda^3$. Taking $p \le \lambda$, $q \le \lambda$ and $t << \lambda$, we ensure that $c << 1$. In order to estimate the Poisson ratio of the composite, we use the simplest mixture rule $\nu = c\nu_i + (1 + c)\nu_m$, where ν_m is the Poisson ratio of the matrix.

Thus, all quantities of Eq. (1) are determined. Let us consider the energy change ΔW in dependence on the dimension and strength of the dislocation loop at relatively low and high temperatures. We take amorphous silicon (Si) and silicon nitride (Si_3N_4) as typical amorphous covalent materials.

3. RESULTS

3.1. Amorphous silicon

In considering the amorphous silicon, we have used its characteristics calculated in computer simulations [22,32,33] at room (T=300K) and higher (T=1000K) temperatures. For room temperature, Demkowicz and Argon [22] have reported the following values of elastic moduli for the solid-like (here matrix) and liquid-like (here inclusion) phases: ($G_m \approx$ 34 GPa, $\nu_m \approx 0.36$) and ($G_i \approx$ 30 GPa, $\nu_i \approx 0.44$). The excess enthalpy of the liquid-like phase of the amorphous material relative to its solid-like phase is given by the difference $H = \Delta H_i - \Delta H_m$, where ΔH_i and ΔH_m are the excess enthalpies of the liquid-like and solid-like phases of amorphous silicon relative to its crystalline state, respectively. Using the data of [22], the latters can be estimated as $\Delta H_i \approx 0.30$ eV/at and $\Delta H_m \approx 0.18$ eV/at at $T \approx$ 300K, in which case we have $H \approx 0.12$ eV/at.

For T = 1000K, we use the same values of elastic moduli as for T = 300K, because they weakly change within the considered narrow range of temperatures. The excess enthalpy H has been estimated on the basis of results of the earlier computer model of Grimaldi et al. [32] (also cited by Spinella et al. [33]). The authors [32] have found the temperature dependences of the excess enthalpy of the amorphous silicon relative to the crystalline silicon for two different amorphous states, relaxed and unrelaxed. Assuming that the relaxed and unrelaxed states of amorphous silicon in computer model of Grimaldi et al. [32] correspond to respectively the solid-like and liquid-like phases of amorphous silicon in computer model of Demkowicz and Argon [22], one can get the estimates $\Delta H_i \approx 0.140$ eV/at and $\Delta H_m \approx 0.095$ eV/at, and therefore $H \approx 0.045$ eV/at at T = 1000K.

For the sake of definiteness, we consider the case of square dislocation loops ($p = q$) and assume that the thickness of the surrounding nucleus of the liquid-like phase (inclusions) increases with the loop extension as $t = b(0.7 + \sqrt[3]{p/b})$, where b

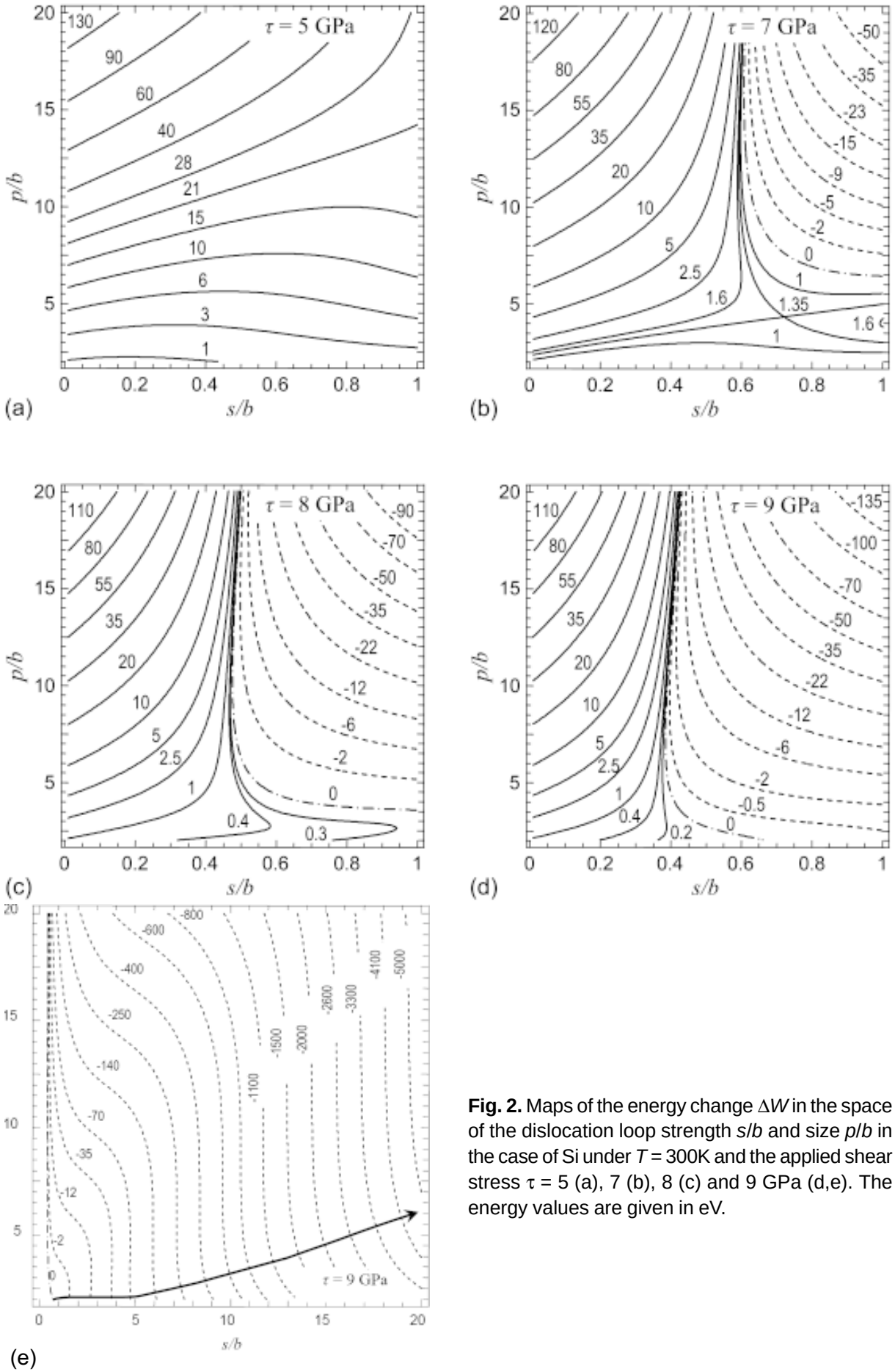

(e)

Fig. 2. Maps of the energy change ΔW in the space of the dislocation loop strength s/b and size p/b in the case of Si under T = 300K and the applied shear stress τ = 5 (a), 7 (b), 8 (c) and 9 GPa (d,e). The energy values are given in eV.

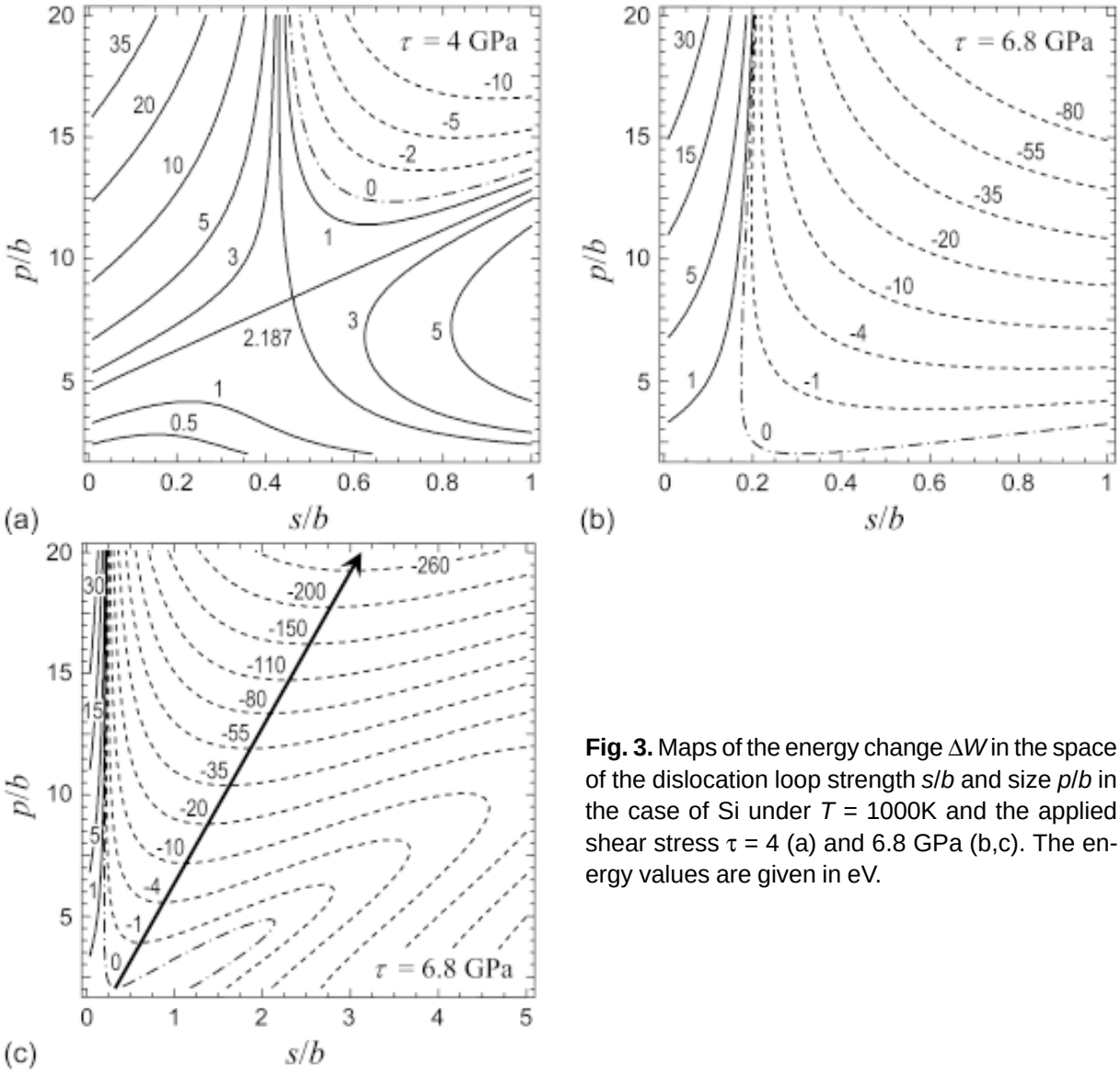

Fig. 3. Maps of the energy change ΔW in the space of the dislocation loop strength s/b and size p/b in the case of Si under T = 1000K and the applied shear stress τ = 4 (a) and 6.8 GPa (b,c). The energy values are given in eV.

≈ 0.27 nm is the average interatomic distance. In this case, at the initial stage of the loop nucleation (at $p \approx 2b$), the inclusion thickness will also be $t \approx 2b$, and further will slowly grow with the loop extension. For the matrix cell dimension $\lambda = 20b$ and the maximum possible size of the loop $p = 20b$, we obtain the inclusion thickness $t \approx 3.4b$. The corresponding maximum volume fraction of inclusion in this model is $c \approx p^2 t/\lambda^3|_{p=\lambda} = t/\lambda \approx 0.17$ which proves the correctness of Eq. (3) for calculating the effective shear modulus of the composite.

The results of numerical calculations, for temperatures 300 and 1000K, are presented in Figs. 2 and 3, respectively, in the form of maps for the energy change ΔW in normalized coordinates s/b and p/b at some different values of the external shear stress τ. When τ is small, the region of negative values of ΔW is separated from the area near the coordinate origin by the region of positive values of ΔW. The region of positive ΔW values images the configuration of the energy barrier for the nucleation of the dislocation loop in coordinates s/b and p/b. The energy barrier reaches its minimum value at the saddle point (see Figs. 2b and 3a). This value is about 1.35 eV (Fig. 2b), for T = 300K and τ = 7 GPa, and about 2.19 eV (Fig. 3a), for T = 1000K and τ = 4 GPa. The corresponding saddle points have the coordinates (0.72, 4.3) and (0.47, 8.4), respectively. Therefore, in the first case, the dislocation loop must grow up to ≈ 4b in size and

≈ 3*b*/4 in strength to overcome the energy barrier. In the second case, these values are $p \approx 8b$ and $s \approx b/2$. Let us estimate the probability of nucleation of such inclusions with dislocation loops under the given temperatures and stresses. As follows from their critical sizes, the number of atoms, which must be involved into the nucleation process, is about $V/b^3 \approx p^2t/b^3$. This gives approximately 37 atoms, for the room temperature, and 200 atoms, for the higher temperature. If one distributes the energy barrier value equally between these atoms, then one gets about 0.038 eV and 0.011 eV in the first and second case, respectively. The average thermal energy kT (where k is the Boltzman constant) per atom is ≈ 0.026eV for T = 300K and ≈ 0.087 eV for T = 1000K. Then, for T = 300K and τ = 7 GPa, the nucleation probability is estimated by ≈ 0.233 per atom and $\approx 3.9 \times 10^{-24}$ per all 37 atoms. For T = 1000K and τ = 4 GPa, the probability is ≈ 0.881 per atom and $\approx 9.9 \times 10^{-12}$ per 200 atoms. One can conclude that the nucleation of inclusions with dislocation loops by means of thermal fluctuations is absolutely impossible under the given temperature and stress conditions.

By increasing the external stress τ, one can cancel the energy barrier in some area of initial values of coordinates *s*/*b* and *p*/*b* (Figs. 2d,e and 3b,c). In the energy map, transition to the barrier-less nucleation corresponds to the situation when the zero-level contour ($\Delta W = 0$) touches the straight line $p = 2b$ related to the initial size of the dislocation loop. This happens when the external stress τ reaches a value about 9 GPa (Fig. 2d,e), for room temperature, and when τ = 6.8 GPa (Fig. 3b,c), for T = 1000K. The touching point has the coordinates about (0.6, 2) in the first case and (0.3, 2) in the second. Therefore, the liquid-like phase inclusion with approximate dimensions $2b \times 2b \times 2b$, which is nucleated in the barrier-less regime, is expected to contain the dislocation loop of strength ≈ 0.6*b*, for T = 300K and τ = 9GPa, and ≈ 0.3*b*, for T = 1000K and τ = 6.8 GPa. The stress values 9 and 6.8 GPa can be considered as critical ones for the barrier-less nucleation of such inclusions and loops at the corresponding temperatures.

Sometimes one can use the energy maps to tailor the most probable evolution of the inclusion and loop under the critical or larger shear stress. The thick arrows in Figs. 2e and 3c, which are drawn from the touching (nucleation) points along the lines of maximum gradient of the function $\Delta W(s,p)$, show how the inclusion and loop develop in the space (s,p) under the corresponding critical stresses. As is seen, they expand, and the strength

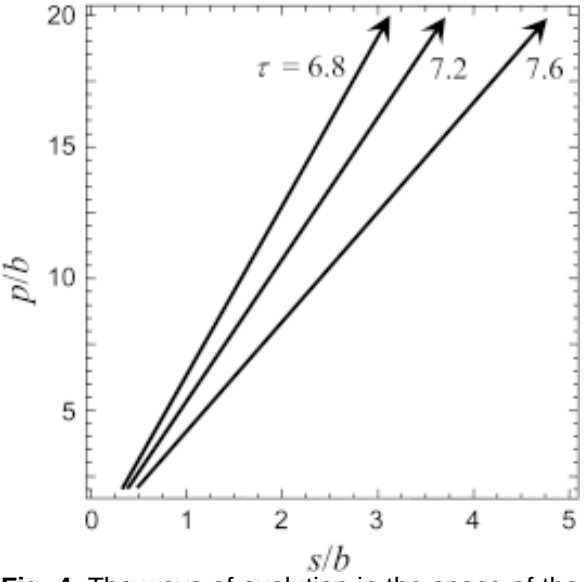

Fig. 4. The ways of evolution in the space of the dislocation loop strength *s*/*b* and size *p*/*b* in the case of Si under T = 1000K and different values of the applied shear stress τ shown at the lines in GPa units.

of dislocation loop simultaneously grows. Unfortunately, in the case of room temperature (Fig. 2e), the line of maximum gradient of $\Delta W(s,p)$ passes through the area $s \geq p$, where formula (2) is not valid, and we can not tailor the system evolution. On the other hand, this line can not go higher, in the field $p>s$, where formula (2) is correct. Therefore, although the evolution path can not be described in detail, we expect that it goes somehow in the area $s \geq p$, in which case the loop strength s increases faster than the loop size p. This situation can be treated as homogeneous nucleation of superdislocation loops (within the liquid-like phase inclusions) whose development results in heterogeneous plastic flow of amorphous silicon, which typically occurs at relatively low temperatures and high external stresses.

In the case of higher temperature, the situation is easy to analyze. The evolution path is represented by a straight arrow (Fig. 3c) which shows that both the inclusion and loop sizes grow faster than the loop strength. In particular, the loop strength s increases from ≈ 0.3*b* to ≈ 3*b* when its size p grows from 2*b* to 20*b*. Thus, under high temperature and critical shear stress, relatively low-strength dislocation loops can homogeneously nucleate and develop by increasing their size and strength. In this situation, one expects occurrence

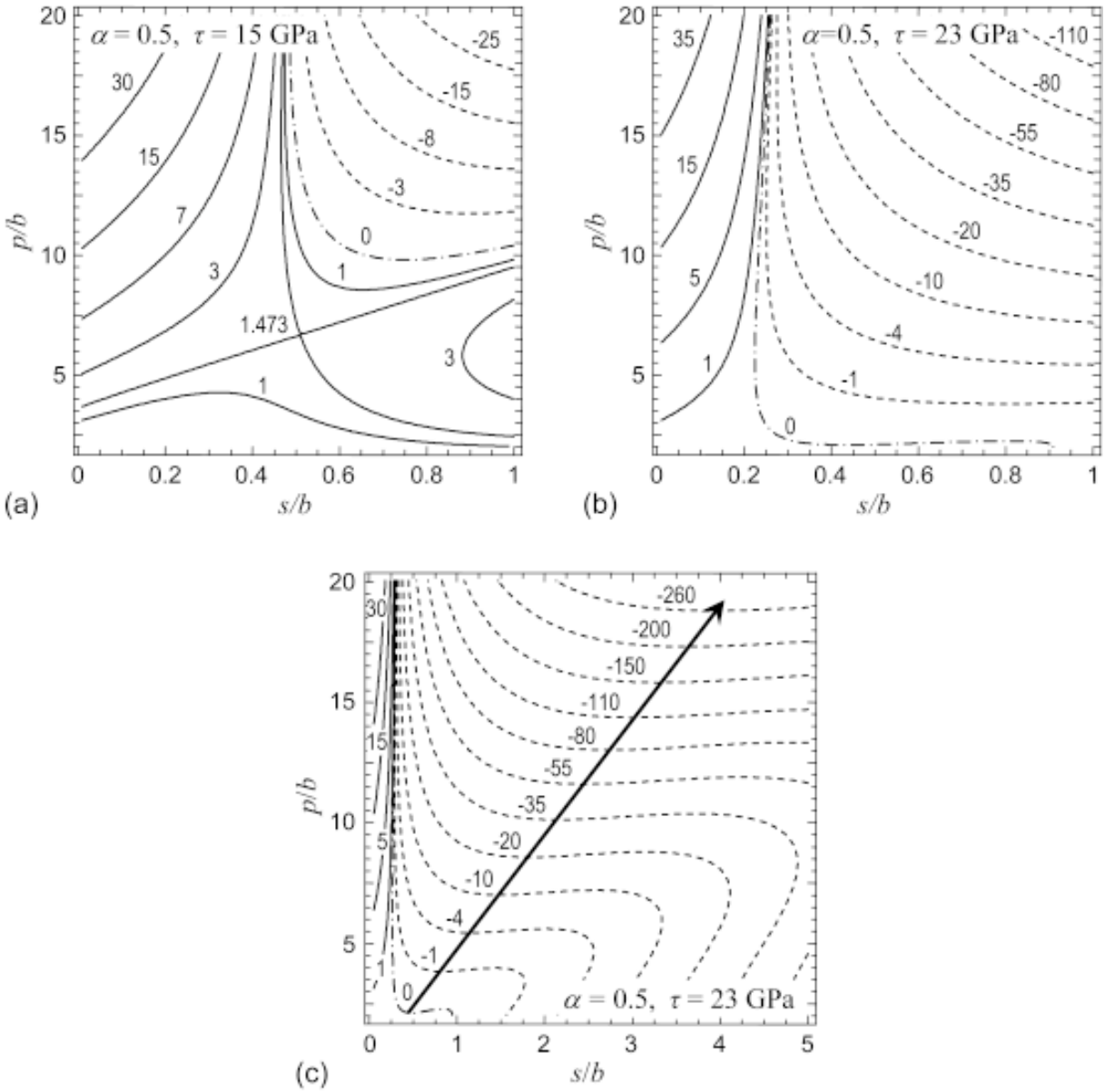

Fig. 5. Maps of the energy change ΔW in the space of the dislocation loop strength s/b and size p/b in the case of Si_3N_4, α = 0.5 and the applied shear stress τ = 15 (a) and 23 GPa (b,c). The energy values are given in eV.

of the homogeneous plastic flow of amorphous silicon by means of both massive nucleation and expansion of such dislocation loops (encapsulated to the liquid-like phase inclusions) over the whole volume of a sample.

The regime of homogeneous plastic flow of amorphous solids is not stable relative to increasing shear stress. The larger stress value stimulates a transition to the heterogeneous regime of plastic flow as demonstrated by atomistic simulation of nanoindentation of amorphous silicon carbide [34]. In terms of our model, this would mean the faster increase in the loop strength s. Indeed, when the applied shear stress τ increases, the slope of evolution path decreases as shown in Fig. 4, which means that the loop strength s grows faster with the loop size p.

3.2. Amorphous silicon nitride

Consideration of the case of amorphous silicon nitride (Si_3N_4) leads to similar conclusions. Unfortunately, this material has not been studied so comprehensively as amorphous silicon at the moment,

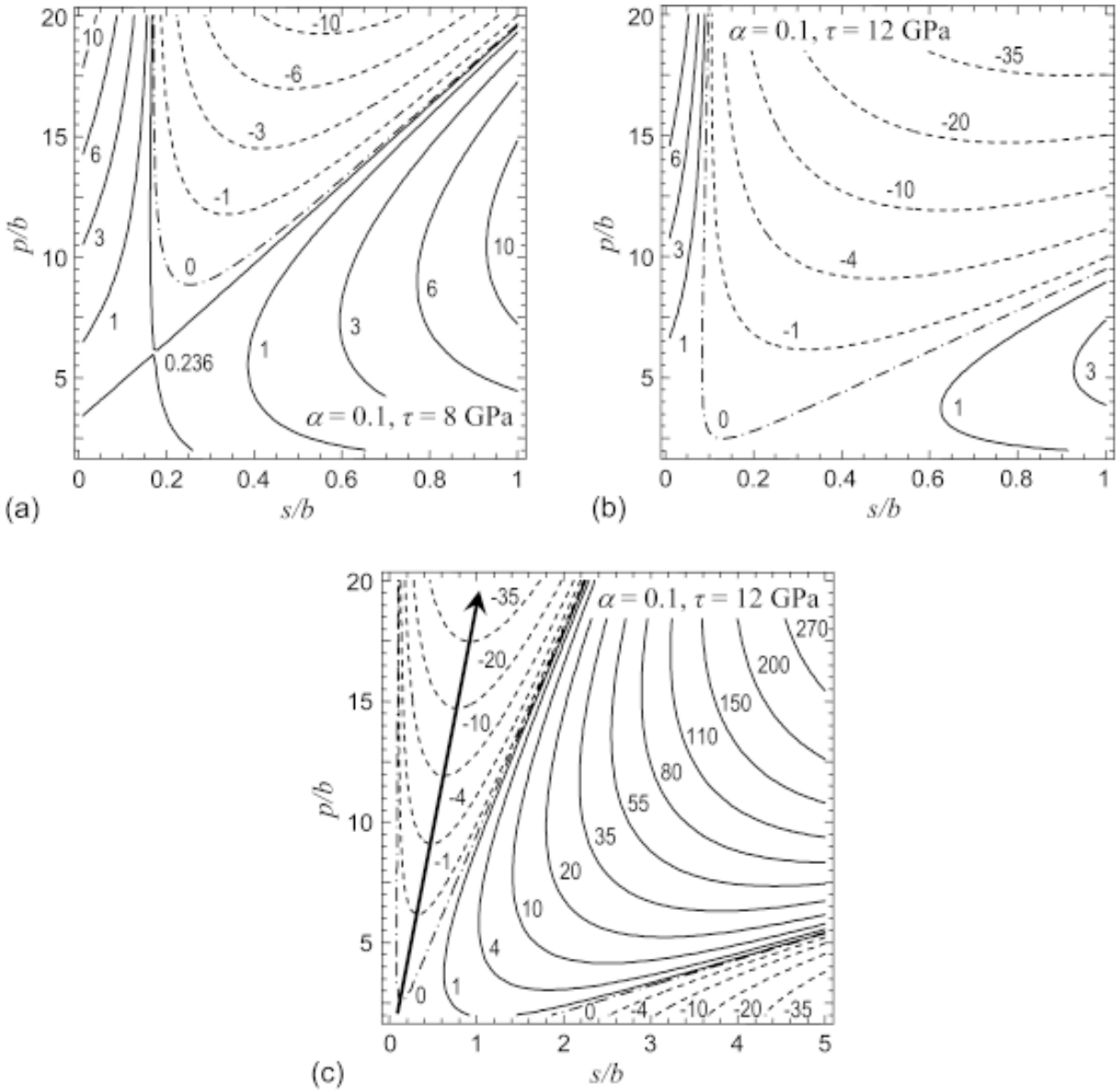

Fig. 6. Maps of the energy change ΔW in the space of the dislocation loop strength s/b and size p/b in the case of Si_3N_4, $\alpha = 0.1$ and the applied shear stress $\tau = 8$ (a) and 12 GPa (b,c). The energy values are given in eV.

and some necessary data are still absent. Therefore we assume that elastic moduli of the liquid-like and solid-like phases of amorphous Si_3N_4 are approximately equal ($G_m \approx G_i \approx G$, $\nu_m \approx \nu_i \approx \nu$) and weakly depend on temperature. Recent precise measurements [35] of the Young modulus E and Poisson ratio ν have shown that $E = 289 \pm 12$ GPa and $\nu = 0.2 \pm 0.05$. Taking the average values, we obtain $G = E/[2(1 + \nu)] \approx 120$ GPa and $\nu \approx 0.2$.

The excess enthalpy H of the liquid-like phase relative to the solid-like phase is supposed to be proportional to the excess enthalpy ΔH_m of the solid-like phase of amorphous Si_3N_4 relative to its crystalline state: $H = \alpha \Delta H_m$, where $\alpha = \alpha(T)$ is a dimensionless parameter depending on temperature. It seems natural to assume that $\alpha << 1$ at high temperatures and $\alpha \leq 1$ at low temperatures. Let us consider two exemplary cases: $\alpha = 0.1$ and 0.5. The magnitude of ΔH_m is estimated [36] by 9.86 kJ/mole of atoms $\approx$ 0.102 eV/at. Thus, we have used two values of H, 0.01 and 0.05 eV/at., in our calculations.

To estimate an average interatomic distance b, which is supposed to be equal to the length of the bond between the closest Si and N atoms, we have utilized the data of experiments [37-39], $b \approx 0.173$-

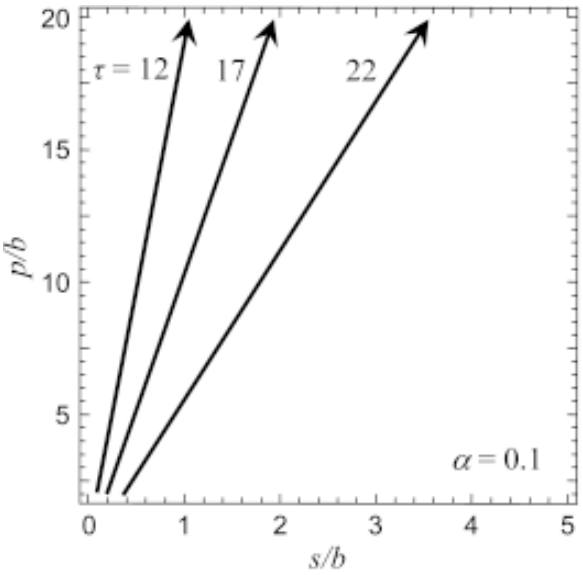

Fig. 7. The ways of evolution in the space of the dislocation loop strength *s*/*b* and size *p*/*b* in the case of Si_3N_4, $\alpha = 0.1$ and different values of the applied shear stress τ shown at the lines in GPa units.

0.175 nm, and computer simulation [40], $b \approx 0.174$-0.176 nm. For calculations, we have taken the average (and the latest [39]) experimental value $b \approx 0.174$ nm.

The results of numerical calculations are demonstrated in Figs. 5 and 6, where the energy maps are shown in the case of $\alpha = 0.5$ (low temperatures) and $\alpha = 0.1$ (high temperatures), respectively. In general, they are similar to the maps given in Fig. 3, although the new maps differ by larger values of the applied shear stress τ as well as by the slopes of the arrowed straights showing the evolution paths of the system.

In the case of $\alpha = 0.5$ (low temperatures, Fig. 5), the critical stress τ_c is about 23 GPa. The nucleus of the liquid-like phase grows in size with simultaneous fast increase in the strength of the dislocation loop: $s \approx 4b$ at $p = 20b$. Therefore, for low temperatures, one expects the plastic flow to occur at a high critical stress, when the liquid-like phase nuclei are formed, grow in size and simultaneously suffer large plastic shears whose magnitudes are in direct proportion with the nucleus sizes. In the given example, $s \approx 0.2p$.

In the case of $\alpha = 0.1$ (high temperatures, Fig. 6), the critical stress τ_c is approximately two times smaller, ≈ 12 GPa, and the nucleus grows in size with a much slower increase of the loop strength: $s \approx b$ at $p \approx 20b$. In other words, for high temperatures, the plastic flow is expected to begin under two times smaller stress, and the nuclei suffer relatively small plastic shears in the process of growth. The shear values remain in direct proportion with the nucleus sizes, although the slope is much smaller here, $s \approx 0.05p$.

Under increasing stress values, the slope of evolution path decreases (Fig. 7), thus demonstrating a step-by-step transition to the heterogeneous regime of plastic flow as with the case of amorphous silicon.

3.3. Nanocomposite *nc*-TiN/a-Si_3N_4 ceramics

Based on the results of the previous section, one can study the processes of plastic flow and crack generation in amorphous intergranular layers of silicon nitride (a-Si_3N_4) which separate nanocrystallites of titanium carbide (*nc*-TiN) in nanocomposite *nc*-TiN/a-Si_3N_4 ceramics.

Let us consider a specimen of such a nanocomposite under a normal tensile stress σ (Fig. 8a) with focuses placed on one of its amorphous interlayers (intergranular boundaries) of length *L* and thickness *h* (Fig. 8b). The interlayer is under the maximum resolved shear stress $\tau = \sigma/2$ (Fig. 8b). It is assumed in the framework of our approach that when the shear stress reaches a critical value $\tau = \tau_c$, a nucleus of the liquid-like phase, which suffers a local plastic shear, is formed in the barrier-less manner (Fig. 8b). The local plastic shear is modeled as a glide dislocation loop of strength ***s***. Under the shear stress τ_c, the nucleus size *p* grows and finally gets the length *L* of the amorphous interlayer (Fig. 8c). At the same time, the loop strength ***s*** grows, too, and gets some value ***B***. Depending on the temperature and stress values, the magnitude of ***B*** can be so large that the dislocation transforms into a superdislocation, that is a dense pile-up of dislocations stopped against the neighboring grain of *nc*-TiN. In the head of this pile-up, a nanocrack of length *l* can be nucleated and propagate along a neighboring amorphous interlayer (Fig. 8c).

The necessary condition for this scenario is given by the inequality $F > 2\gamma$ [41], where *F* is the energy release rate (the strain energy released when a crack propagates over a unit distance) and γ is the specific surface energy of the interlayer material. The equation $F = 2\gamma$ determines two characteristic lengths of the crack: (i) its equilibrium length l_{eq}, if $\partial F/\partial l|_{l=l_{eq}} < 0$, and (ii) its critical (Griffith's)

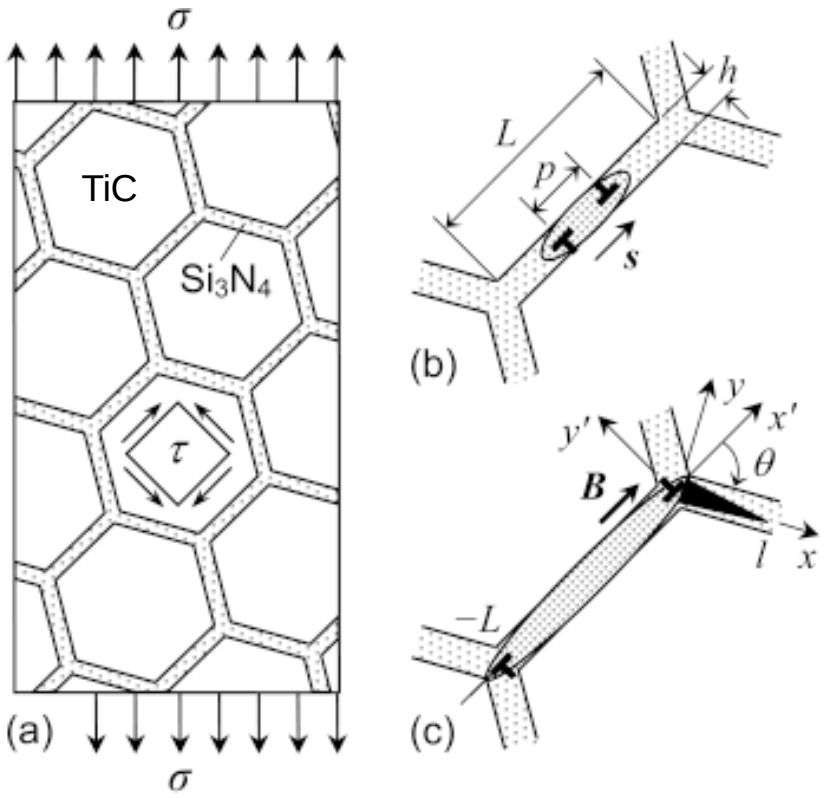

Fig. 8. Model of plastic flow and crack nucleation within intergranular layers of amorphous Si_3N_4 in nanocomposite *nc*-TiN/*a*-Si_3N_4 ceramics. (a) A model specimen of the nanocomposite under an applied tensile stress σ. (b) Nucleation and development of a local shear event in *a*-Si_3N_4 interlayer is treated as a glide dislocation loop of strength (Burgers vector) ***s***, which is surrounded by an ellipsoidal region of liquid-like phase. (c) The superdislocation loop of an increased strength ***B*** reaches the triple junctions of neighboring *a*-Si_3N_4 interlayers and causes the nucleation of a crack of length l in one of them.

length l_c, if $\partial F/\partial l|_{l=l_c} > 0$. In dependence on the stressed state of the region, where the crack is nucleated and grows, there are some possibilities for its development. First, the crack can be nucleated and grow in the barrier-less regime if the condition $F > 2\gamma$ is valid for any $l > l_0$, where l_0 is some minimal crack length (of the order of some interatomic distances) at which the notion of a crack has its sense [42]. Second, the crack can be nucleated and grow in the barrier-less regime only until its equilibrium length l_{eq} if $F > 2\gamma$ and $\partial F/\partial l < 0$ for $l_0 < l < l_{eq}$ [41,42]. Third, the classical Griffith's [43] case is realized when the crack must overcome an energy barrier at its length l_c to be nucleated and grow further if $F > 2\gamma$ and $\partial F/\partial l > 0$ at $l_0 \le l_c < l$. Fourth, there exists a combination of the second and third cases where the crack is nucleated and grows in the barrier-less regime up to the length l_{eq}. After that, the crack can grow further under the conditions of overcoming the energy barrier and reaching the critical length l_c. If the criterion $F > 2\gamma$ is not valid at any length of the crack, one can guarantee that crack generation is impossible in such stress field. Within our model, this means that, instead of crack generation, the plastic flow in the neighboring amorphous interlayers of the nanocomposite is expected to occur.

Let us use the criterion $F > 2\gamma$ to estimate the conditions necessary for generation of a nanocrack in our model (Fig. 8c). In doing so, we take into account the fact that the elastic moduli of *nc*-TiN and *a*-Si_3N_4 are rather close. Indeed, the Young modulus and Poisson ratio of the nanocomposite ceramics are $E \approx 350$ GPa and $\nu \approx 0.25$ [44], respectively, and therefore the shear modulus is $G \approx 140$ GPa. The latter is rather close to the shear modulus $G \approx 120$ GPa of the *a*-Si_3N_4 (see Section 3.2). Thus, in the first approximation, we consider the nanocomposite *nc*-TiN/*a*-Si_3N_4 ceramics as an

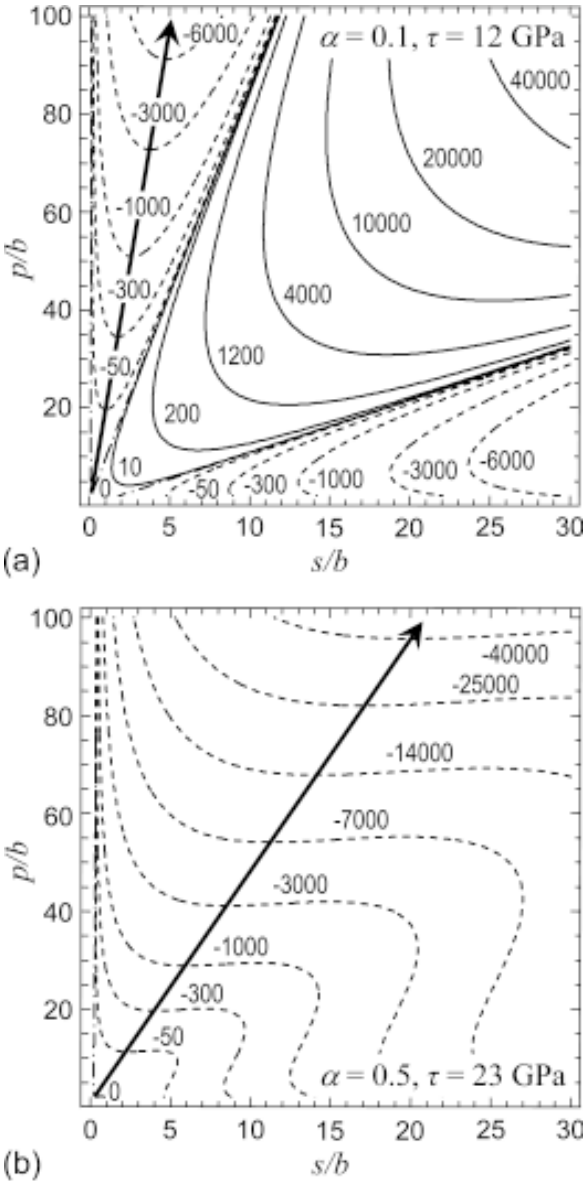

Fig. 9. Maps of the energy change ΔW in the space of the dislocation loop strength *s*/*b* and size *p*/*b* in the case of Si_3N_4; (a) $\alpha = 0.1$ and $\tau = 12$ GPa, and (b) $\alpha = 0.5$ and $\tau = 23$ GPa. The energy values are given in eV.

elastically homogeneous isotropic material with the elastic moduli $G \approx 140$ GPa and $\nu \approx 0.25$.

For the sake of simplicity, we will use the following two-dimensional model. We take a cylinder with the elliptic cross section instead of the oblate ellipsoid for the shape of the liquid-like phase nucleus, and a dipole of straight edge dislocations with the Burgers vectors ± ***s*** instead of the glide dislocation loop. Let the dipole arm *p* grow up to the interlayer length *L* (Fig. 8c). Within the above energetic approach, one can estimate the corresponding magnitude of ***s***, which is hereinafter called *B*. For definiteness we take $L = 100b$ that with $b \approx 0.174$ nm gives $L \approx 17$ nm, the typical average length of amorphous interlayers in the nanocomposite *nc*-TiN/*a*-Si_3N_4 ceramics. The maps of the energy change ΔW for the cases of $\alpha = 0.1$ and $\tau_c = 12$ GPa (high temperatures, Fig. 9a) and $\alpha = 0.5$ and $\tau_c = 23$ GPa (low temperatures, Fig. 9b) show that $B \approx 5b \approx 0.87$ nm for high temperatures and $B \approx 21b \approx 3.65$ nm for low temperatures. It is worth noting that the evolution paths remain straight as before: $B \approx 0.05L$ for high temperature and $B \approx 0.2L$ for low temperature.

Following Indenbom [41], the energy release rate *F*, in the case shown in Fig. 8c, can be calculated as follows

$$F = \frac{l}{8D}\left(\overline{\sigma}_{yy}^{2} + \overline{\sigma}_{xy}^{2}\right), \tag{4}$$

where $D = G/[2\pi(1 - \nu)]$ and $\overline{\sigma}_{iy}$ is the average weighted stress (i=x,y) which acts in the segment ($0 \le x \le l$, $y = 0$):

$$\overline{\sigma}_{iy} = \frac{2}{\pi l}\int_0^l \sigma_{iy}(x, y=0)\sqrt{\frac{x}{x-l}}\,\mathrm{d}x. \tag{5}$$

Here the stress σ_{iy} is a superposition of the dislocation stress $\sigma_{iy}^{(d)}$ and the applied stress $\sigma_{iy}^{(ex)}$: $\sigma_{iy}=\sigma_{iy}^{(d)}+\sigma_{iy}^{(ex)}$.

In the coordinate system (x',y') related to the interlayer plane (Fig. 8c), the stress components of the dislocation dipole are [45]

$$\sigma_{x'x'}^{(d)} = -DBy'\left\{\frac{3x'^2 + y'^2}{\left(x'^2 + y'^2\right)^2} - \frac{3\left(x'+L\right)^2 + y'^2}{\left[\left(x'+L\right)^2 + y'^2\right]^2}\right\}, \tag{6}$$

$$\sigma_{y'y'}^{(d)} = DBy'\left\{\frac{x'^2 - y'^2}{\left(x'^2 + y'^2\right)^2} - \frac{\left(x'+L\right)^2 - y'^2}{\left[\left(x'+L\right)^2 + y'^2\right]^2}\right\}, \tag{7}$$

$$\sigma_{x'y'}^{(d)} = DB\left\{\frac{x'\left(x'^2 - y'^2\right)}{\left(x'^2 + y'^2\right)^2} - \frac{\left(x'+L\right)\left[\left(x'+L\right)^2 - y'^2\right]}{\left[\left(x'+L\right)^2 + y'^2\right]^2}\right\}. \tag{8}$$

Using the transforms of coordinates, x' = $x\cos\theta + y\sin\theta$ and $y' = -x\sin\theta + y\cos\theta$, and stress components,

$$\sigma_{yy} = \frac{1}{2}\left(\sigma_{x'x'} + \sigma_{y'y'}\right) - \frac{1}{2}\left(\sigma_{x'x'} - \sigma_{y'y'}\right)\cos 2\theta + \sigma_{x'y'}\sin 2\theta, \quad (9)$$

$$\sigma_{xy} = \frac{1}{2}\left(\sigma_{x'x'} - \sigma_{y'y'}\right)\sin 2\theta + \sigma_{x'y'}\cos 2\theta, \quad (10)$$

we obtain the normal and shear stresses which act in the plane of the nucleating crack:

$$\sigma_{yy}^{(d)}(x, y=0) = DB\sin\theta\left\{\frac{1}{x} - \frac{x}{x^2 + 2xL\cos\theta + L^2} - 2L\frac{\left(x^2 - L^2\right)\cos\theta + xL\sin^2\theta}{\left(x^2 + 2xL\cos\theta + L^2\right)^2}\right\}, \quad (11)$$

$$\sigma_{xy}^{(d)}(x, y=0) = DB\left\{\frac{\cos\theta}{x} - \frac{x\cos\theta + L}{x^2 + 2xL\cos\theta + L^2} - L^2\frac{(\cos 2\theta - 1)(x\cos\theta + L)}{\left(x^2 + 2xL\cos\theta + L^2\right)^2}\right\}, \quad (12)$$

$$\sigma_{yy}^{(ex)} = \tau(1 + \sin 2\theta), \quad (13)$$

$$\sigma_{xy}^{(ex)} = \tau\cos 2\theta. \quad (14)$$

Introducing these stresses to the integral in Eq. (5), we find the average weighted stresses which can be written as

$$\overline{\sigma}_{iy}^{(d)} = \frac{DB}{l}\sqrt{\frac{L}{c}}f_{iy}\left(\tilde{L}, \theta\right), \quad (15)$$

$$\overline{\sigma}_{iy}^{(ex)} = \sigma_{iy}^{(ex)}, \quad (16)$$

where

$$f_{yy} = 2\sin\left(\theta + \frac{\varphi}{2}\right) + \sin\frac{\varphi}{2}\left\{\tilde{h}\left(\tilde{h} + 2\tilde{L} - 1\right)\cdot(1 - \cos\varphi) + \left[\left(\tilde{L}^2 - 1\right)\cot\theta\csc\theta - \tilde{L}\right]\cdot(2 - \cos\varphi - \cos 2\varphi)\right\}, \quad (17)$$

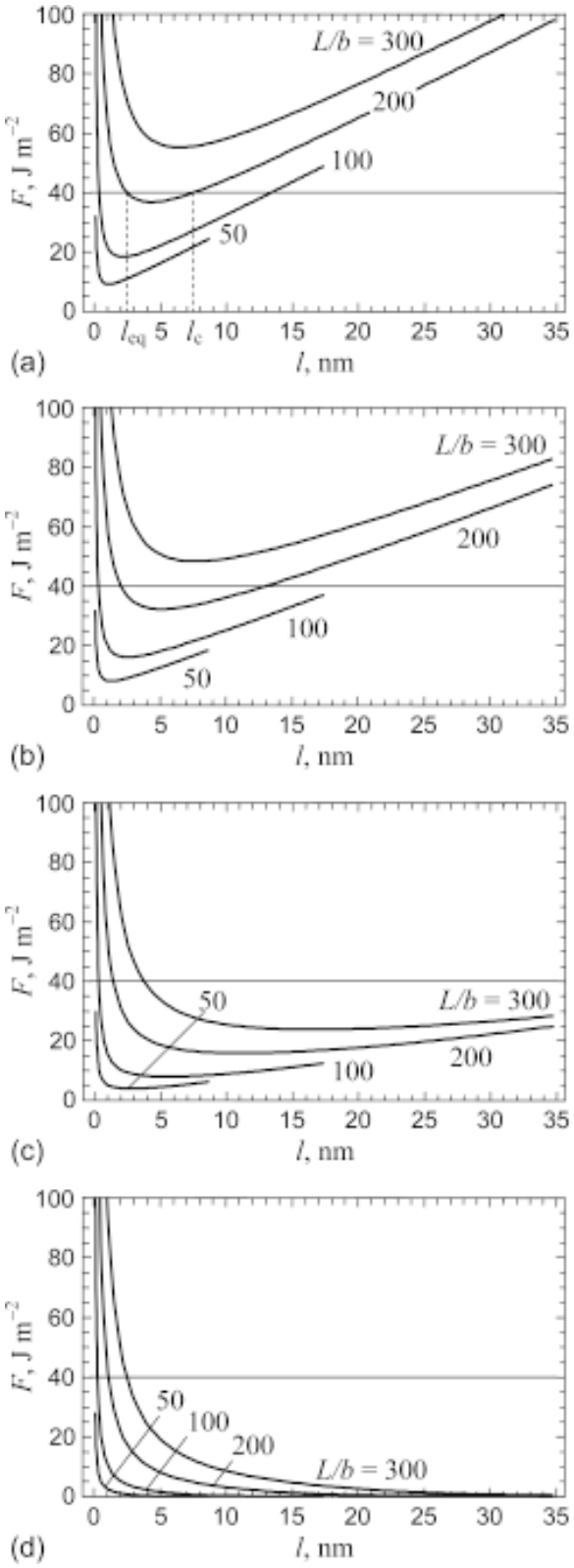

Fig. 10. Dependence of the energy release rate F on the crack length l, for different lengths L of the a-Si_3N_4 interlayer (shown at the curves), at $\alpha = 0.1$, $\tau = 12$ GPa, and $\theta = 45°$ (a), 75° (b), 105° (c), and 135° (d). The horizontal line shows the surface energy level $2\gamma = 40$ J m^{-2}.

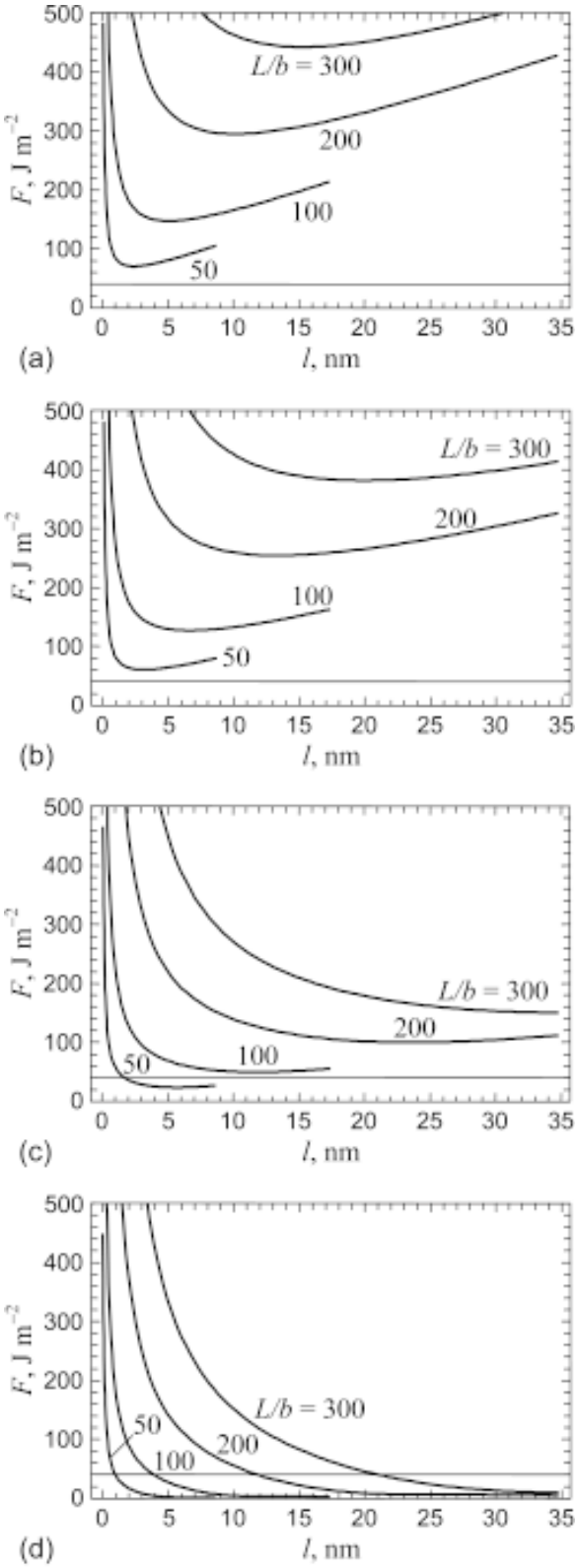

Fig. 11. Dependence of the energy release rate F on the crack length l, for different lengths L of the a-Si_3N_4 interlayer (shown at the curves), at $\alpha = 0.5$, $\tau = 23$ GPa, and $\theta = 45°$ (a), 75° (b), 105° (c), and 135° (d). The horizontal line shows the surface energy level $2\gamma = 40$ J m^{-2}.

$$f_{xy} = 2\cos\left(\theta + \frac{\varphi}{2}\right) + \sin\frac{\varphi}{2}\csc\theta\left\{\tilde{h}\right.$$
$$\cdot\left(\tilde{h} + 2\tilde{L} + \cos\theta\right)(1 - \cos\varphi) + \tilde{L}\left(\tilde{L} + \cos\theta\right) \quad (18)$$
$$\left.\cdot(2 - \cos\varphi - \cos 2\varphi)\right\},$$

and the following denotations are used: $\tilde{L} = L/l$, $\tilde{h} = h/l$, $h = \sqrt{L^2 + 2Ll\cos\theta + l^2}$, $\varphi = \arcsin(\sin\theta/\tilde{h})$.

With Eqs. (15)-(18), the energy release rate F reads

$$F = \frac{DB}{8}\left\{\frac{BL}{lc}\left(f_{yy}^2 + f_{xy}^2\right) + \frac{2\tau}{D}\sqrt{\frac{L}{c}}\right.$$
$$\cdot\left[f_{yy}(1 + \sin 2\theta) + f_{xy}\cos 2\theta\right]$$
$$\left. + \frac{2l\tau^2}{BD^2}(1 + \sin 2\theta)\right\}. \quad (19)$$

Let us consider the validity of criterion $F > 2\gamma$ at high ($B \approx 0.05L$) and low ($B \approx 0.2L$) temperatures of testing of our model specimen. Unfortunately, we have failed to find in literature any reliable data on the value of γ for a-Si_3N_4 interlayers. Therefore, we take the estimate $\gamma = 20$ J m^{-2} which has been utilized by Tsurula et al. [46] in computer simulations of crack growth in nanoamorphous Si_3N_4 under room temperature. There is also no information concerning the temperature dependence of γ. Based on the changes in the surface energy of ceramic Si_3N_4 specimens, which are composed of crystalline micro- and nanograins separated by amorphous interlayers, one can state that in the range of moderate temperatures ($T < 1400$K), the γ value is weakly changed, diminishing with T within 30% [47]. In the range of higher temperatures, γ can grow fast [47-49]. For definiteness, we assume in our calculations that γ is constant ($\gamma = 20$ J m^{-2} [46]), keeping in mind that in the case of high temperatures this will give us the upper estimate for the equilibrium length l_{eq} of the crack and the under estimate for its critical length l_c.

The dependence of the energy release rate F on the crack length l, for different values of the dipole arm (interlayer length) L and the crack orientation angle θ, is shown in Figs. 10 (high temperatures, $B \approx 0.05L$) and 11 (low temperatures, $B \approx 0.2L$).

In the case of high temperature, the validity of criterion $F > 2\gamma$ strongly depends on the interlayer length L and the orientation angle θ (Fig. 10). For relatively small angles [here $\theta = 45°$ (Fig. 10a) and

75° (Fig. 10b)], the main factor is the length L which is proportional to the average size of the crystallite (grain) d: $d \approx 2L$. When L is relatively large (here $L = 300b \approx 52$ nm and $d \approx 100$ nm), the criterion $F > 2\gamma$ is valid for any crack length l. This means that there exist not energy barriers in the framework of the present model, and the crack growth is energetically favorable. When L is a bit smaller (here $L = 200b \approx 35$ nm and $d \approx 70$ nm), the criterion $F > 2\gamma$ is valid for very small crack length $l < l_{eq}$ (here $l_{eq} \approx 2.5$ nm at $\theta = 45°$ and ≈ 2 nm at 75°) and relatively large crack length $l > l_c$ (here $l_c \approx 7.5$ nm at $\theta = 45°$ and ≈ 13 nm at 75°). A crack of intermediate length $l_{eq} \le l \le l_c$ would be energetically unfavorable. When L is medium (here $L = 100b \approx 17$ nm and $d \approx 35$ nm), the equilibrium length of the crack becomes so small ($l_{eq} < 0.5$ nm) that one can not account for it. At the same time, its critical length l_c approaches the interlayer length ($l_{eq} \approx 13.5$ nm at $\theta = 45°$, Fig. 10a) or even exceeds it (at $\theta = 75°$, Fig. 10b). Therefore, the probability of crack generation abruptly drops here. Finally, when L is very small (here $L = 50b \approx 9$ nm and $d \approx 17$ nm), the criterion $F > 2\gamma$ is not valid, and the crack generation is impossible within our model.

At high temperature and relatively large angle θ [here $\theta = 105°$ (Fig. 10c) and 135° (Fig. 10 d)], only very short cracks can be generated in between large and medium nanograins. For large L, the equilibrium crack length l_{eq} is about 4 and 2.5 nm at $\theta = 105°$ and 135°, respectively; for medium L, it is approximately 1.5 and 1 nm (of the order of the minimal possible crack length l_0), respectively. At the same angles and smaller grain size, the crack generation is impossible.

In the case of low temperature, the situation drastically changes (Fig. 11). At relatively small angles [here $\theta = 45°$ (Fig. 11a) and 75° (Fig. 11b)], the criterion $F > 2\gamma$ is valid for any grain size, that is, the crack generation and its unlimited growth are barrier-less and energetically favorable. At medium angles (here $\theta = 105°$) and very small grain sizes (here $L = 50b \approx 9$ nm and $d \approx 17$ nm), only very short cracks (here with $l_{eq} \approx 1.7$ nm) can be generated, while at the larger grain sizes (here $d \ge 35$ nm), the barrier-less nucleation and unlimited growth of cracks are still possible. At large angles (here $\theta = 135°$) and any grain size, the crack growth is limited by its equilibrium length: $l_{eq} \approx 4$, 12 and 21 nm, for $L \approx 17$, 35 and 52 nm ($d \approx 35$, 70 and 100 nm), respectively. When the grain size is very small, one can state that the crack is not generated because its equilibrium length $l_{eq} \approx 1$ nm is either smaller than or of the same order as l_0.

Thus, at low temperature of testing, our model sample of nanocomposite *nc*-TiN/*a*-Si_3N_4 ceramics is subject of cracking in much higher degree than at high temperature. Within the model, it is caused by much higher level of applied shear stress τ necessary for the formation of nuclei of liquid-like phase in amorphous interlayers, and by significantly larger Burgers vectors of the superdislocations stopped by the triple junctions of the interlayers. It is shown that the interlayer length L (and therefore, the grain size d) exerts a strong influence upon the possibility of crack generation in amorphous interlayers. A decrease in L (refinement of nanograins) leads to diminishing of both the superdislocation Burgers vector and dipole arm, in which case the dislocation stresses greatly decrease. As a result, the energy release rate F decreases as well, and the validity of criterion $F > 2\gamma$ can be violated. This is quite evident in the case of high temperatures (Fig. 10) when the value of F is commensurate with the fracture energy 2γ. At low temperatures, the value of F in the most cases is significantly larger than the estimate $2\gamma = 40$ J m^{-2} [36] used in calculations (Fig. 11). Assuming that this estimate is not exact and might be some times larger, one can expect a strong influence of the grain size upon the cracking at low temperature, too. Our conclusion that grain refinement can prevent the intergranular cracking well corresponds to the experimental result that hardness of the columnar nanocomposite *nc*-TiN/*a*-SiN_x coatings noticeably increases when the grain diameters decreases in the range from 100…150 nm to 20 nm [50,51].

4. SUMMARY

We have suggested a theoretical model describing plastic flow in covalent amorphous solids and amorphous intergranular boundaries in nanoceramics. Based on atomic simulations of Demkowicz and Argon [21-23], it is supposed that the nuclei of liquid-like phase are formed and grow in size within solid-like matrix phase under an external load. These nuclei suffer plastic shears modeled through glide dislocation loops which are generated inside the nuclei and develop together with them. Energetics of the formation and growth of the nuclei has been studied in detail with application to bulk amorphous silicon and silicon nitride, and amorphous intergranular layers of silicon nitride which separate nanocrystallites of titanium carbide in nanocomposite *nc*-TiN/*a*-Si_3N_4 ceramics. It is shown that when the applied shear stress

reaches a critical value, the formation and growth of the nuclei become energetically favorable. The critical stress value strongly depends on temperature; the higher critical stress corresponds to the lower temperature. Moreover, under low temperatures, the strength (Burgers vector magnitude) of the dislocation loop, which describes the plastic shear inside a nucleus, grows faster than under high temperatures. This means that under low temperatures and relatively large applied stresses, one expects the heterogeneous plastic flow which is realized through generation and propagation of several nuclei of liquid-like phase containing dislocation loops of high strength. Since these nuclei are strong sources of elastic strains, they can stimulate heterogeneous generation of new nuclei in the shear plane, thus leading to the formation of powerful shear bands. In the opposite case of high temperatures and relatively small applied stresses, one expects the homogeneous plastic flow which is realized through multiple generation and extension of many liquid-like phase nuclei with dislocation loops of low strength. The important issue is that if the applied stress exceeds the critical value, which is characteristic of the given high temperature, the dislocation strength grows faster, and the homogeneous regime of plastic flow can be replaced by the heterogeneous regime that is in accordance with results of atomic simulations of Szlufarska et al. [34].

We have also proposed a theoretical model which demonstrates that the nucleation and development of liquid-like phase nuclei within intergranular layers of *a*-Si_3N_4 in nanocomposite *nc*-TiN/*a*-Si_3N_4 ceramics can stimulate crack generation in the neighboring *a*-Si_3N_4 interlayers. By using the energy approach, we have investigated the necessary conditions for the barrier-less and energetically favorable nucleation of mixed (I and II) mode nanocracks under the stresses due to superdislocation dipoles and external loading. The equilibrium and critical crack lengths have been calculated and studied in dependence on the temperature, grain size, and crack orientation. Our model shows that nanocomposite *nc*-TiN/*a*-Si_3N_4 ceramics are inclined to intergranular cracking in much higher degree at low temperature and large grain size than at high temperature and small grain size.

ACKNOWLEDGEMENTS

The work was supported, in part, by the Russian Foundation of Basic Research (Grants 08-01-00225-a and 08-02-00304-a), the Russian Academy of Sciences Program “Fundamental studies in nanotechnologies and nanomaterials”, the Office of Naval Research (grant N00014-07-1-0295), and the National Science Foundation Grant CMMI #0700272.

REFERENCES

[1] A.K. Mukherjee // *Mater. Sci. Eng. A* **322** (2002) 1.
[2] M.Yu. Gutkin and I.A. Ovid’ko, *Plastic Deformation in Nanocrystalline Materials* (Springer, Berlin, 2004).
[3] H. Klostermann, F. Fietzke, T. Modes and O. Zywitzki // *Rev. Adv. Mater. Sci.* **15** (2007) 33.
[4] M. Balden, C. Adelhelm, T. Köck, A. Herrmann and J. Jaimerena-Muga // *Rev.Adv.Mater.Sci*. **15** (2007) 95.
[5] A. Akbari, J.P. Riviere, C. Templier, E. Le Bourhis and G. Abadias // *Rev. Adv. Mater. Sci*. **15** (2007) 111.
[6] A.M. Saad, V.A. Kalaev, J.A. Fedotova, K.A. Sitnikov, A.V. Sitnikov, Yu.E. Kalinin, A.K. Fedotov and V.A. Svito // *Rev. Adv. Mater. Sci.* **15** (2007) 208.
[7] T. Polcar, A. Nossa, M. Evaristo and A. Cavaleiro *// Rev. Adv. Mater. Sci.* **15** (2007) 118.
[8] I.A. Ovid’ko and A.G. Sheinerman // *Rev.Adv.Mater.Sci*. **16** (2007) 1.
[9] A. Swiderska-Sroda, G. Kalisz, B. Palosz and N. Herlin-Boime // *Rev. Adv. Mater. Sci.* **18** (2008) 422.
[10] T. Yamasaki, H. Yokoyama and T. Fukami *// Rev. Adv. Mater. Sci*. **18** (2008) 711.
[11] S. Veprek and A.S. Argon // *J. Vac. Sci. Technol*. **20** (2002) 650.
[12] G.-D. Zhan, J.D. Kuntz, J. Wan and A.K. Mukherjee // *Nature Mater.* **2** (2003) 38.
[13] G.-D. Zhan, J.D. Kuntz and A.K. Mukherjee // *MRS Bull*. **29** (2004) 22.
[14] Y.T. Pei, D. Galvan and J.T.M. De Hosson // *Acta Mater*. **53** (2005) 4505.
[15] X. Jin, L. Gao and J. Sun // *Acta Mater***. 54** (2006) 4035.
[16] X. Xu, T. Nishimura, N. Hirosaki, R.-J. Xie, Y. Yamamoto and H. Tanaka // *Acta Mater***. 54** (2006) 255.
[17] D.M. Hulbert, D. Jiang, J.D. Kuntz, Y. Kodera and A.K. Mukherjee // *Scripta Mater*. **56** (2007) 1103.

[18] C.C. Koch, I.A. Ovid'ko, S. Seal and S. Veprek, *Structural Nanocrystalline Materials: Fundamentals and Applications* (Cambridge University Press, Cambridge, 2007).
[19] I. Szlufarska, A. Nakano and P. Vashishta // *Science* **309** (2005) 911.
[20] Y. Mo and I. Szlufarska // *Appl. Phys. Lett.* **90** (2007) 181926.
[21] M.J. Demkowicz and A.S. Argon // *Phys. Rev. Lett.* **93** (2004) 025505.
[22] M.J. Demkowicz and A.S. Argon // *Phys. Rev. B* **72** (2005) 245205.
[23] M.J. Demkowicz and A.S. Argon // *Phys. Rev. B* **72** (2005) 245206.
[24] M.J. Demkowicz, A.S. Argon, D. Farkas and M. Frary // *Phil. Mag*. **87** (2007) 4253.
[25] A.S. Argon // *Acta Metall.* **27** (1979) 47.
[26] M. Yu. Gutkin, T. Ishizaki, S. Kuramoto and I.A. Ovid'ko // *Acta Mater.* **54** (2006) 2489.
[27] M. Yu. Gutkin and I.A. Ovid'ko // *Appl. Phys. Lett*. **88** (2006) 211901.
[28] M. Yu. Gutkin and I.A. Ovid'ko // *Acta Mater.* **56** (2008) 1642.
[29] J.P. Cui, Y.L. Hao, S.L. Li, M.L. Sui, D.X. Li and R. Yang // *Phys. Rev. Lett*. **102** (2009) 045503.
[30] M. Yu. Gutkin, I.A. Ovid'ko and Yu.I. Meshcheryakov // *J. Phys. III* (France) **3** (1993) 1563.
[31] R.M. Christensen, Mechanics of Composite Materials (Wiley, New York, 1979).
[32] M.G. Grimaldi, P. Baeri and M.A. Malverazzi // *Phys. Rev.* B **44** (1991) 1546.
[33] C. Spinella, S. Lombardo and F. Priolo // *J. Appl. Phys*. **84** (1998) 5383.
[34] I. Szlufarska, R.K. Kalia, A. Nakano and P. Vashishta // *Appl. Phys. Lett*. **86** (2005) 021915.
[35] A. Khan, J. Philip and P. Hess // *J. Appl. Phys*. **95** (2004)1667.
[36] R.F. Zhang and S. Veprek // *Phys. Rev.* B **76** (2007) 74105.
[37] T. Aiyama, T. Fukunaga, K. Niihara, T. Hirai and K. Suzuki // *J. Non-Cryst. Solids* **33** (1979) 131.
[38] M. Misawa, T. Fukunaga, K. Niihara, T. Hirai and K. Suzuki // *J. Non-Cryst. Solids* **34** (1979) 313.
[39] T. Fukunaga, T. Goto, M. Misawa, T. Hirai and K. Suzuki // *J. Non-Cryst. Solids* **95-96** (1987) 1119.
[40] P. Ordejón and F. Ynduráin // *J. Non-Cryst. Solids* **137-138** (1991) 891.
[41] V.L. Indenbom // *Phys. Sol. State* **3** (1961) 1506.
[42] I.A. Ovid'ko and A.G. Sheinerman // *Acta Mater*. **52** (2004) 1201.
[43] A.A. Griffith // *Phil. Trans. Roy. Soc. London A* **221** (1921) 163.
[44] R.G. Veprek, D.M. Parks, A.S. Argon and S. Veprek // *Mater. Sci. Eng. A* **422** (2006) 205.
[45] J.P. Hirth and J. Lothe, *Theory of Dislocations* (Wiley, New York, 1982).
[46] K. Tsurula, A. Nakano, R.K. Kalia and P. Vashishta // *J. Am. Ceram. Soc.* **81** (1998) 433.
[47] R.W. Trice and J.W. Halloran // *J. Am. Ceram. Soc*. **82** (1999) 2633.
[48] Y.P. Zeng, J.F. Yang, N. Kondo, T. Ohji, H. Kita and S. Kanzaki // *J. Am. Ceram. Soc.* **88** (2005) 1622.
[49] X. Zhu and Y. Sakka // *Sci. Technol. Adv. Mater*. **9** (2008) 033001.
[50] F. Kauffmann, B.H. Ji, G. Dehm, H.J. Gao and E. Arzt // *Scr. Mater*. **52** (2005) 1269.
[51] C. Lu, Y.W. Mai and Y.G. Shen // *J. Mater. Sci.* **41** (2006) 937.